Vol. 13(1), pp. 1-17, January-June, 2023
DOI: 10.5897/JOMS2019.0157
Article Number: C80E8F670306
ISSN: 2141-2294

http://www.academicjournals.org/JOMS

ACADEMIC JOURNALS
expand your knowledge

Journal of Oceanography and Marine Science

Full Length Research

Hurricane latent heat energy from annual Amazon deforestation runoff

Frederick Kenneth Weiersmueller

University of Missouri, St. Louis, 1 University Blvd. St. Louis, Missouri 63121-4400, United States.

Received 19 November 2019; Accepted 20 March, 2022

This study analyzed latent heat flux from Amazon deforestation runoff above the Central/North American Boundary currents from 1988-2015. The purpose is to propose Atlantic hurricane intensification from the heat flux via condensation. The author divided those currents into ten areas of evaporation considering water budget data and regional and water-vapor-transport. A spreadsheet program consisting of two models had three inputs. Evaporation in each of the ten areas became the first input. For simplicity, each area's evaporation decremented incoming runoff one time, and passed through less runoff, considering the currents' average velocities and ocean condensation residency. Recent high-flow runoff data, limited from June 1 through November 30, a typical hurricane season, became the other inputs: all Amazon runoff (Model-A), only Amazon deforestation runoff (Model-O). The spreadsheet converted the condensation heat flux from each season (km3) into 10^17 J/day. This study compared those values to the 10^17 J/day wind energy of Category-1 or Category-3 hurricanes, finding order of magnitude similarity for such a crude comparison. The author then correlated hurricane Emily's July 2005 daily path interface with the daily latent heat flux from the deforestation runoff. The analysis indicated that daily heat flux interfacing with Emily's path measured 5.82% of a Category-3's 10^17 J/day. When considering reuse runoff in deforested areas aggregate from 1970 to 2004, that 5.82% increases to possibly 12.85%. This study's simple analysis is by like terms (J/day) and similar order of magnitude (10^17) only, necessitating a more complex analysis.

Key words: Deforestation, hurricanes, latent heat flux, modelling, runoff.

INTRODUCTION

Recent estimates illustrate the historic costs and potential energy of Atlantic hurricanes. In 2005, Hurricane Katrina cost $161 billion (NOAAFastFacts, 2013). In 2012, Sandy caused $18.75 billion in insured property losses alone (Artemis, 2013) and $65 billion in total cost. In 2005 Emily became the earliest-forming Category-5 hurricane on record for the month of July in the Atlantic basin (Franklin and Brown, 2006). Considering the prevention of human and dollar costs, a study indicates Rapid Intensification (RI) of hurricanes is notoriously difficult to predict and can contribute to severe destruction and loss of life (Balaguru et al., 2018). Studies have categorized the intensity of these hurricanes by their maximum wind speed. A Category-1 rating requires a one-minute-

*Corresponding author. E-mail: fkweiers@gmail.com.

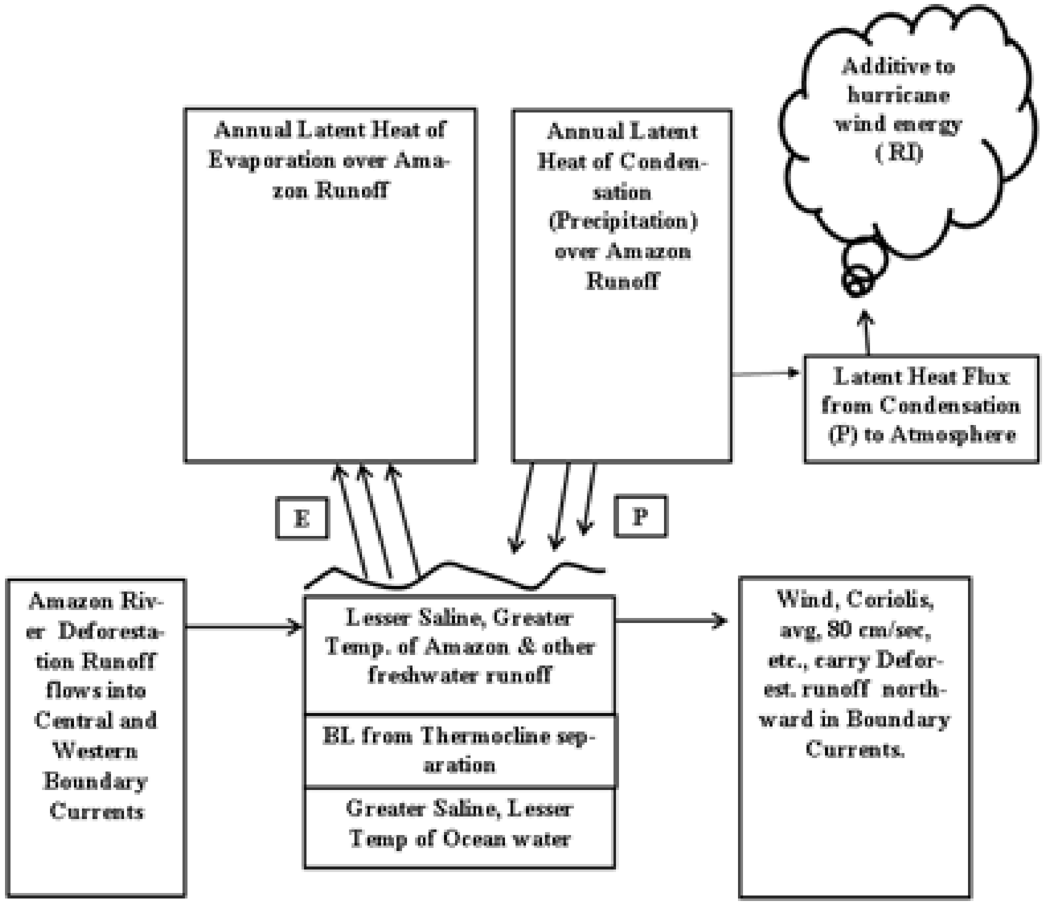

Figure 1. Amazon River deforestation runoff latent heat flux additive to hurricanes.
Source: Frederick Kenneth Weiersmueller

average maximum sustained winds at 10 m above the surface of 33-42 m/s, a Category-3 requires 50-50 m/s (Saffir and Simpson, 1973).

Several model simulations demonstrated the Amazon runoff's Rapid Intensification (RI) of North Atlantic hurricanes. One earlier study (Vizy and Cook, 2010) using atmospheric models identified how the Amazon River plume's presence increases the stability of the Barrier Layer (BL) near the surface water. This allowed warm Sea Surface Temperature (SST) anomalies to increase the number of tropical storms reaching hurricane strength by 61%. A later study (Balaguru et al., 2012), illustrated the relationship between SST increase from the BL formed by Amazon River discharge region and more accurately simulated the tropical Atlantic atmosphere. Recently, another study (Gouveia et al., 2019) proposed a conceptual model showing the influence of Amazon runoff increase and its impact on the SST. That model indicated warming of the amazon plume, thereby influencing latent flux heat to the tropical Atlantic atmosphere. However, these SST studies are limited in that they find no quantified anthropogenic cause for the RI of Atlantic hurricanes. This study drills down to one specific and significant anthropogenic cause for RI– Amazon deforestation runoff. Figure 1 summarizes this study.

The comparisons herein are by like terms and similar order of magnitude only, noting that Emanuel, (1998) indicates large quantities of latent heat flux are necessary to perform work on the air. Nonetheless, this study attempts to quantify the deforestation runoff latent heat flux missing from the literature. Regarding that Amazon deforestation runoff, a source reports almost all precipitation over deforested rainforest (e.g. Amazon) is lost as runoff (Raven and Berg, 2006). That is due in large part to the impervious nature of the upper plinthic soil in the Amazon rainforest. Two Amazon rain forest studies reported this: northern Para, Brazil (Chaves et al., 2008) and in southern Rondonia, Brazil (de Moraes et al., 2006). After that Amazon deforestation runoff flows into its discharge plume it becomes part of the North Brazil Current, the first of the boundary currents analyzed here. The aim of this study is to calculate the actual latent heat flux volumes from that deforestation runoff in the Central/North American Boundary currents. In addition, this study shows when and where those heat flux volumes

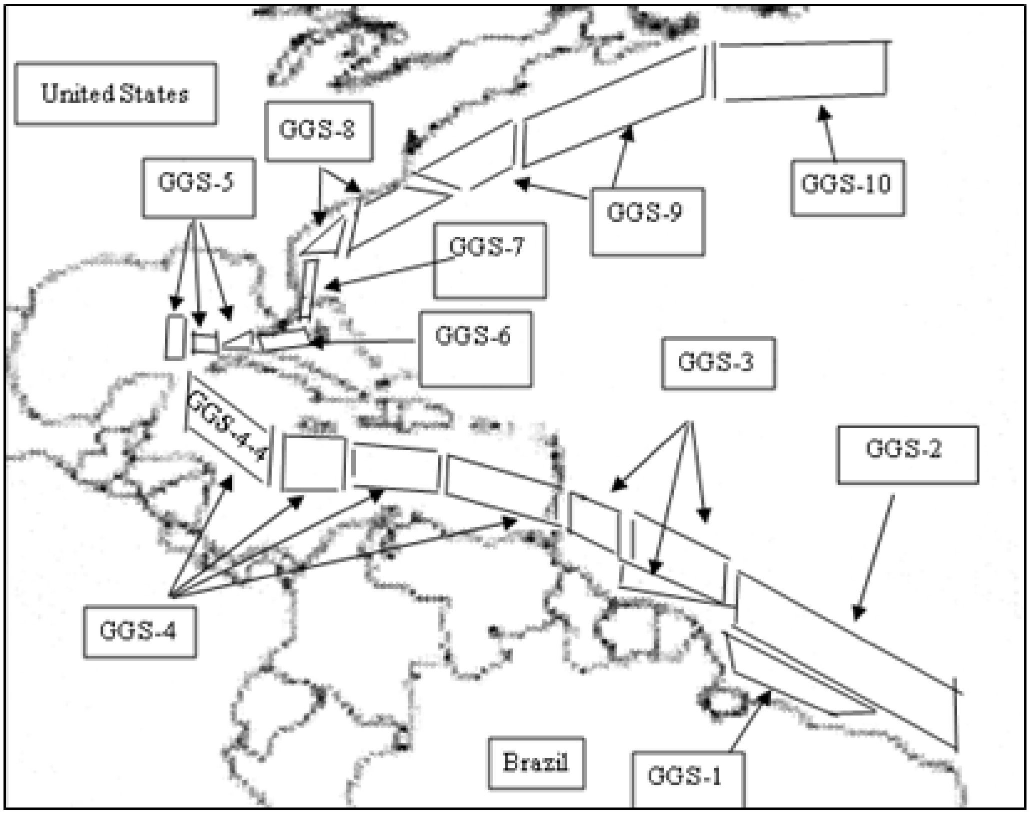

Figure 2. Approximate Greater Gulf Stream (GGS) currents after www.outline-world-map.com.
Source: Frederick Kenneth Weiersmueller

may have intersected a recent hurricane's path. It also converts those volumes into hurricane wind- energy terms to see what percentage they are of a typical hurricane's wind-energy. It does that considering the whole of the Central/North American Boundary currents as well as the individual currents. In this way, the author hopes to show the mechanisms linking Amazon River deforestation runoff to the Rapid Intensification (RI) of Central/North American Boundary current hurricanes.

METHODOLOGY

This study utilizes an Excel spreadsheet program, using MS Office Version 14.0.7015.1000. Henceforth it will refer to the spreadsheet program simply as "Spreadsheet". Latent Heat of Condensation Potential Energy (LHCPE) refers to flux from Model-A Amazon runoff and from Model-O Amazon runoff. The author refers to the ten main divisions of the Central/North American Boundary currents in Figure 2, as the Greater Gulf Stream (GGS). The GGS includes the Amazon discharge plume (GGS-1), North Brazil (GGS-2), Guiana (GGS-3), Caribbean Sea (GGS-4), Loop (GGS-5), Florida (GGS-6 & GGS-7) currents. The GGS also includes the northern part of the traditional Gulf Stream (GGS-8, GGS-9, and GGS-10). Some GGS-n are divided into geometric GGS-n-n subdivisions. The Mariano (2016) website maps indicate these currents with curvy arrows of one-degree longitude/latitude (MarianoArrowData, 2013). This study approximates the distance between these arrows as 100 km, latitude or longitude (WikipediaLongitude, 2019). The author estimates 162 traversal days for a hypothetical runoff floater in GGS-1 to reach the GGS-10 endpoint, based on 11,200 km approximate distance northward, at a typical GGS velocity of 80 cm/sec (Mariano, 2016). Dividing each GGS geometric surface areas by the known global ocean surface area, 361.9 × 10^6 km^2 (Eakins and Sharman, 2010), yields a ratio, the Surface Area Coefficient (SAC). The SAC factor assists in calculating the annual evaporation over each GGS current. Supplementary Materials Item A, (SMA), details the SAC geometric factor calculations for all ten GGS currents. This study assumes 7 days residence for evaporation over oceans and 8.9 days over land after (van der Ent and Tuinenburg, 2017).

Spreadsheet section A – Factors and GGS evaporation

The SAC factor provides a good point to introduce the Spreadsheet, which has a matrix with three sections: Section A (factors and GGS evaporation), Section B (Model-A) and Section C (Model-O). That matrix is the source for most of the tables, figures, and SMa herein. Figure 3 illustrates Section A of the 2005 Spreadsheet iteration. The Section A values are constant for all the 1988-2015 Spreadsheet iterations. The SAC factor in column C becomes a variable in the columns F and G formulas. Additionally, two other latitudinal factors effect calculations of evaporation. First, this study developed the Regional Evaporation Coefficient (REC) factor by the author's interpolation. after Wunsch (2005) Figure-3-Right. That figure details the Northern hemisphere atmospheric residual heat flux in Petawatts (PW), see SMB. This provided a

Model A vs. Model O: Amazon River Runoff Volumes of Evaporation, Latent Heat and Atmospheric E ner

		Section A						
2005 (km3)		**Annual Evaporation Data Over GGS Currents**					**Only Jun1 - Nov30 Evaporation**	**R**
Column Formulas [1]		**factors**			**C x D x 413k**	**C x E x 40k**	**(F - G) x 0.5**	
A	**B**	**C**	**D**	**E**	**F**	**G**	**H**	
Formula Yield Desc. [1]		**GGS Surf. Area Coef-ficient (SAC)**	**GGS Reg. Evap. Coef-ficient (REC)**	**GGS Evap. Trans-fer Inland Cycl. Ratio**	**Initial Evap. Over Surf. Area**	**Evap. Transfer back into Con-tinent**	**Long Term Evap. over Surf. Areas**	
[5]	**[5]**	**[5]**	**[6]**	**[2]**		**[2]**	**[2]**	
		[3] Initial Runoff Inputs (Jun - Nov) -->						
	1	0.000166	-0.20	0.75	-13.73	4.99	-9.36	
	2	0.001994	-0.20	0.75	-164.74	59.83	-112.29	
	3	0.000997	0.80	0.70	329.48	27.92	150.78	
	4	0.002216	1.60	0.13	1464.38	11.08	726.65	
GGS	5	0.000332	2.90	0.35	398.13	4.65	196.74	
	6	0.000055	3.00	0.30	68.64	0.66	33.99	
	7	0.000024	3.10	0.25	31.03	0.24	15.39	
	8	0.000665	3.70	0.25	1015.91	6.65	504.63	
	9	0.001042	4.15	0.18	1786.35	7.30	889.53	
	10	0.001330	4.20	0.20	2306.39	10.64	1147.88	
Totals:					7222	133.96	3544	

Figure 3. 2005-Spreadsheet Iteration – Section A
Source: Frederick Kenneth Weiersmueller

basis for the Regional Evaporation Coefficient (REC) factors in column D of Figure 3. The REC factor becomes a variable in the column F formula. Second, this study developed the Evaporation Transfer Inland Cycling Ratio by the author's interpolation after van der Ent and Savenije (2013) , see SMC. This provides the basis for that ratio in Column E Figure 3, which accounts for water vapor transport inland variations. The latitudinal variance data in that study only covered the period 1990–2009. However, another study (de Moraes et al., 2006) using the Earth system model GFDL-ESM2G, indicates only a 3% increase in the Ocean to Land Water Vapor Transport between the end of the 20th century (1999) and the end of the 21st century (2099). That is only 0.18% increase for the six years data, 2010-2015, missing in van der Ent and Savenije, 2013) study. Therefore, the author used van der Ent and Savenije (2013) latitudinal ratios for the REC factor over the complete 1988-2015 timeframe. The ratio becomes a variable in column G formula. Columns F and G formulas also utilize the water budget data factors (Trenberth et al., 2007), that is, Ocean Evaporation of 413/year and Ocean Evaporation Transfer Inland of 40k km^3/year. Also, Model-A and Model-O utilize the factor of Ocean Precipitation of 373k km^3/year (Trenberth et al., 2007).

Spreadsheet sections B and C – Model-A and Model-O

Figure 4 illustrates the 2005 Spreadsheet iteration for column H of Section A, and all of Section B, and Section C. The Spreadsheet contains several bracketed numbers "[n]" that help pinpoint certain cells, columns, or rows. Note [1] refers to the Column Formulas row and the Formula Yield Descriptions row. Note [2] refers to Evaporation Transfers Inland Cycling Ratios for each current. Note [3] indicates Initial Runoff (Jun - Nov) input into the discharge plume for both Model-A and Model-O. Note [3] also refers to the runoff leaving each successive GGS current. Note [4] refers to the first type of Spreadsheet proportional expression, "L x Mprev/Iprev"; that is, Model-O-Evaporation equals Model-A-Evaporation times the ratio of Model-O runoff to Model-A runoff; Note [5] refers to GGS current numbering and SAC factor. Note [6] refers to REC factor for all GGS-n currents. Note [7] refers to the second type of Spreadsheet proportional expression containing the ratio of condensation-to-evaporation 373k/413k (Trenberth et al., 2007) in Sections B and C; and [7] also refers to the phenomenon – when ocean water vapor condenses (precipitation) the latent heat releases to the surrounding atmosphere, and the water molecules

	Section B - Jun1-Nov30			Section C - Jun1-Nov30			
Only Jun1 - Nov30 Evaporation	Model A: Amazon River Runoff			Model O: Only Amazon River Defororestation Runoff			
	Runoff Exhaustion	Latent Heat		Long Term Evap.	Runoff Exhaustion	Latent Heat	
(F - G) x 0.5	I prev - H	H x 373k / 413k	H - J	H x M prev / I prev	M prev - L	L x 373k / 413k	L - N
H	I*	J**	K***	L****	M*	N**	O***
Long Term Evap. over Surf. Areas	Initial, then Volume Leaving GGS Current after LT Evap.	Latent Heat of Cond. PE to Atmos. (LHCPE)	Latent Heat of Evap. Residue in Atmos.	Long Term Evap. over Surf. Area	Initial, then Volume Leaving GGS Current after LT Evap.	Latent Heat of Cond. PE to Atmos. (LHCPE)	Latent Heat of Evap. Residue in Atmos.
[2]	[3]	[7]	[7]	[4]	[3]	[7]	[7]
	2555				4.13		
-9.36	2564.0973	-8.4511	-0.9063	-0.0151	4.1413	-0.0136	-0.0015
-112.29	2676.3854	-101.4127	-10.8754	-0.1814	4.3226	-0.1638	-0.0176
150.78	2525.6043	136.1777	14.6035	0.2435	4.0791	0.2199	0.0236
726.65	1798.9561	656.2706	70.3775	1.1736	2.9055	1.0599	0.1137
196.74	1602.2192	177.6824	19.0544	0.3178	2.5877	0.2870	0.0308
33.99	1568.2303	30.6970	3.2919	0.0549	2.5329	0.0496	0.0053
15.39	1552.8354	13.9039	1.4910	0.0249	2.5080	0.0225	0.0024
504.63	1048.2038	455.7568	48.8747	0.8150	1.6930	0.7361	0.0789
889.53	158.6748	803.3761	86.1529	1.4367	0.2563	1.2975	0.1391
1147.88	0.0001	143.3068	15.3680	1.8539	0.0001	0.2315	0.0248
3544		2307				3.73	

Figure 4. 2005-Spreadsheet – Sections B & C (also Col. H, Sect. A).
Source: Frederick Kenneth Weiersmueller

return to the ocean (Lindsey, 2009; Met, 2021). This leaves some lessor evaporative flux residue. The Spreadsheet column-labels I through O, have asterisk suffixes. Like-numbered asterisks indicate a similar IF-THEN-ELSE formula logic, not displayed in the Column Formula row. For example, column-labels "I*" and "M*", Equation 1 and 2 respectively, prevent circular reference and division by zero. They involve columns Q and R as memory cells off the main worksheet, not shown in Figure 4. Thus, any GGS-n zero-result in Sections B and C is expressed by a four-digit decimal number, "0.0001". That number indicates exhaustion of a GGS-n's runoff by evaporation; and it prevents circular reference and division by zero.

=IF(Q22<=0,0.0001,SUM(I21-H22)) (1)

=IF(R22<=0,0.0001,SUM(M21-L22)) (2)

The column labels with two, three and four asterisks have more-involved IF-THEN-ELSE logic. Their purpose is the correct accounting of evaporative/condensation values once runoff exhaustion occurs in the previous GGS-n current and results in a value of "0.0001".

The calculation of Model-A Initial Runoff Input in Figure 4 is 2555 km^3, column I. To arrive at that initial input volume, the author has annotated lines onto Figure 5a and 5b after Giffard P, et al. (2019).

Calculation of Amazon Model-A Initial Runoff (Jun-Nov).

First, Figure 5a indicates the Amazon flow-rate varies during the year. The author annotated parallel lines onto Figure 5a, for the June 1 through November 30 seasonal Amazon runoff (Goldstein, 2021). The author approximated that hashed-area as 45% of the ISBA annual runoff. The Giffard et al. (2019) study employed two data sets: ISBA satellite measurements and HYBAM Obidos-station gauge measurements. In Figure 5b, the interannual measurements of the HYBAM data (1993-2015) partially correlated to ISBA data (1970-2015). The Giffard et al. (2019) study reported that where the years overlapped in the two data sources, the HYBAM data corresponded. Also, the ISBA data correlated well with the 1988-2019 annual deforestation data from another study (INPE, 2019) for Model-O calculations. Therefore, this study used the ISBA-CTRIP data to calculate the Initial Runoff (Jun - Nov) values. Interestingly, the Amazon runoff flow is almost three times greater during the rainy season (0.275 × 10^6 m^3/s, May-Jun) than during the dry season (0.10 × 10^6 m^3/s, Dec-Jan). Second, Figure 5b indicates Amazon runoff flow-rate varies interannually. In Figure 5b, the author has annotated vertical/horizontal lines and small circles to interpolate the Amazon runoff interannual data. For the 2005 interpolation, the author converted the values to10^12 m^3/year, using the 31.54 × 10^6 s per year SI units conversion factor. This yields 5677 km^3 for Jan-Dec, and after applying the 45% factor, yields 2555 km3 runoff. That becomes the Spreadsheet 2005

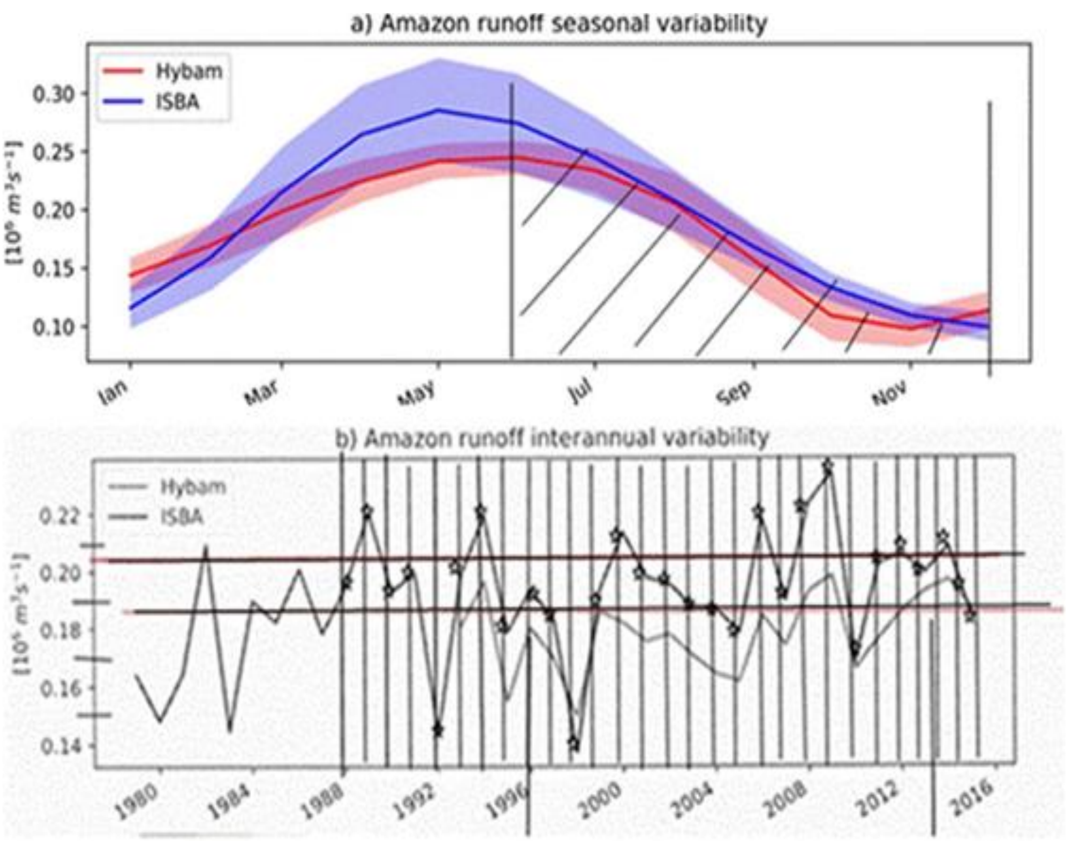

Figure 5. (a) Annotation (hash area) after of Giffard et al. (2019), Figure 4a, Jun-Nov. (b) Annotations (lines/circles) after Giffard et al. (2019).

Model-A “Initial Input Runoff (Jun - Nov):” in column I, that is, runoff received by GGS-1. The Spreadsheet accounted for this calculation regarding the other 1988-2015 iterations in the same manner.

Calculation of Amazon Initial Model-O deforestation runoff (Jun-Nov)

Turning to Section C, the Model-O Initial Runoff Input is 4.13 km^3 in column M of Figure 4. For that data, the author utilized the annual deforestation satellite data (INPE, 2019), (PRODES Amazon, 2020). For 2005, those sources indicate yearly deforestation area of 19,014 km^2 or 19.0 × 10^9 m^2 (INPE, 2019). To calculate the deforestation runoff, this study utilized a factor from another study (Bruno et al., 2006) - Amazon rainforest has 0.53 m^3 water holding capacity per m^3 of soil, nearly uniform with soil depth. Therefore, taking conservatively the upper one meter of soil from Bruno (2006), then 0.53 m^3 of water per m^2 of soil exists over the 19.0 x 10^9 m^2 of deforested soil. That yields 10.07 × 10^9 m^3 water or 10.07 km^3. Therefore, as in Model-A, applying the 45% factor (Giffard et al., 2019) yields 4.53 km^3 for the June through November 2005 deforested runoff input, up to this point.

However, the author considered two smaller factors that restrict that 4.53 km^3 Model-O yield, namely the exoreic evaporation and groundwater losses. Model-A accounted for these two factors in its Obidos station data. The Amazon Basin contains 6.3 × 10^6 km^2 (Goulding et al., 2003), a fraction of the 149 × 10^6 km^2 global land area, that is, glaciers, habitable land, beaches, dunes, exposed rocks, salt flats, deserts (Ritchie and Rose, 2019), or 4.2%. Also, a World Water Resources monogram finds 2100 km^3/year direct global groundwater runoff to the ocean and 1100 km^3/year global exoreic evaporation (Shiklomanov, 1998). Applying the 4.2% factor yields 88.2 km^3 of groundwater exited directly to ocean and 46.2 km^3 of exoreic evaporation occurred from the Amazon Basin. In addition, the Amazon Basin totaling 6.3 × 10^6 km^2 (Goulding et al., 2003) received 19,014 km^2 (INPE, 2019) deforestation in 2005, or 0.3%. This study established earlier that deforested land returns most precipitation to runoff (Chaves et al., 2008), (de Moraes et al., 2006). Therefore, after applying the 0.3% factor, the yields are 0.14 km^3 of exoreic evaporation and 0.26 km^3 of groundwater direct to ocean from the Amazon Basin 2005 deforested area. Thus, 4.53 km^3 minus 0.14 km^3 exoreic minus 0.26 km^3 groundwater yields 4.13 km^3, the 2005 Model-O “Initial Input Runoff (Jun - Nov):” in column M, received by GGS-1. The Spreadsheet accounted for this calculation regarding the other 1988-2015 iterations, see SME for details.

Conversion of Model-O LHCPE km3 to 10^17 J/day in Table 1.

The 2005 Spreadsheet iteration calculated 3.73 km3 Model-O-GGS-LHCPE at the bottom of column N in Figure 4, cumulative from the GGS-n components. Table 1 details the Spreadsheet conversion of 2005 LHCPE from seasonal km3 into 10^17 J/day. This study maintains that atmospheric potential energy, LHCPE, resides in the atmosphere ahead of the path of the hurricane. And it maintains the LHCPE is additive, intensifying existing hurricane

Table 1. Conversion of Model-O LHCPE km^3 to 10^17 J/day, see SMC for 2569 kJ/kg determination.

Spreadsheet 2005 Model-O LHCPE conversion to J/day and its comparison to hurricane wind energies calculated by NHC and Emanuel (1998)							
A	B	C	D	E	F	G	H
Sprdsht km^3/seas. = 10^12 kg (1cc=1 g, $H_2$0)	YYYY	Jun-Nov tot. km^3 conv. to	C x 2569 kJ/kg	D x 10^3 J/kJ	E / 180 (ea. day Jun-Nov)	F conv. to	G conv. to
		10^12 kg/seas.	10^12 kJ/seas.	10^12 J/seas.	10^12 J/day	10^17 J/day	10^19 J/day
LHCPE to Atmos.	2005	3.73	9582.37	9582370	53235.39	0.53	0.0053
Evap. Residue.	2005	0.39	1001.91	1001910	5566.17	0.06	0.0006
NHC Method 1							5.2
NHC Method-2						1.3	
Emanuel KA (1998)						2.6	

Source: Frederick Kenneth Weiersmueller

wind energy causing category changes through condensation in the hurricane's concentric outer rain-bands. This study compares that LHCPE potential energy to studies of hurricane wind energy from two other studies. Those are: the NHC Method-2 study of wind energy (NHC, 2020; Emanuel, 1998) for Category-1, and the non-NHC study (Emanuel, 1998) for Category-3. Those two studies calculate the daily wind energy by integrating the hurricane dissipation that occurs mostly in the atmospheric surface layer area covered by a circularly symmetric hurricane.

The NHC Method-1 (NHC, 2020; Gray, 1981) for an average hurricane or Category-1 was not considered for this study. The NHC Method-1 calculated total energy released through the volumetric cloud/rain formation, from the eyewall to the outer radius of a hurricane. There are any number of concentric rain-bands that radiate out from the eyewall, interspersed with non-rainbands (Zehnder, 2020). Another study (de Moraes et al., 2006) using radar reflectivity data, found that the distant rainbands contain the deep convective cores and they typically mature or die by the time they reach the inner core. Therefore, this study assumes LHCPE added its potential heat energy to the atmosphere earlier in the outermost rain-bands, before they spiral inward. For completeness, Table 1 lists the much larger NHC Method-1 calculation.

RESULTS

The author considered Table 1 2005 demonstration a crude comparison, nevertheless finding order of magnitude similarity in regards to hurricane RI, and will attempt to refine the comparison here. Henceforth, unless otherwise specified, "LHCPE" refers to the Model-O-LHCPE in the "Totals:" Spreadsheet row, calculated from Jun-Nov deforestation runoff. Figure 6 graphs the INPE (km^2) raw deforestation data from 1988-2015 before the Bruno (2006) factor, 0.53 m^3/m^2, and the Giffard et al. (2019) factor, 45% of annual, are applied. Two averages illustrate significant differences in Figure 6: the raw 1988-2008 INPE average of 17,690 km^2 versus the 2009-2015 INPE average of 6,086 km^2. It is interesting to note that the raw deforestation data for 2016-2020 has begun an upswing: 7,900, 6900, 7500, 10,100 and 10,900 km^2, respectively (INPE, 2019). The average for this five-year upsurge is 8660 km^2. That is 30% more than the 2009-2015 low average of 6086 km^2. Figure 7 graphs the Spreadsheet LHCPE (km^3) output from the Jun-Nov INPE deforestation runoff input to the 1988-2015 Spreadsheet iterations. SME lists the 1988-2015 Spreadsheet iteration results in more detail. The 19,014 km^2 raw data from 2005 was converted to 4.13 km^3 input to the Spreadsheet. That resulted in 3.73 km^3 of Jun-Nov LHCPE. Figure 7 echoes the 1988-2008 versus the 2009-2015 difference in LHCPE averages seen in Figure 6 in terms of seasonal INPE averages. Noteworthy, is a high mark 29,100 km^2 in 1995, which resulted in 5.71 km^3 of seasonal LHCPE. It compares to the low mark of 4600 km^2 in 2012, which resulted in only 0.90 km3 of seasonal LHCPE. Next, this study looked at Hurricane Emily's 2005 path through any specific GGS-n(-n) areas and its wind speeds along that path.

Hurricane Emily's path and wind speed through GGS-4 in 2005

Figure 8 contains the best track and wind speeds of Emily with annotations after (Franklin and Brown, 2006). The report indicates Hurricane Emily formed at roughly 0112 UTC 14 July approximately 85 n mi east-southeast of Grenada (very eastern end of GGS-4-1). The author's annotations on Figure 8a, illustrate that Emily traversed the entire GGS-4 area The author's annotations on Figure 8b illustrate Emily's wind speed during that time. Emily was a Category-3 or greater during approximately 87% of the time from 0112 UTC 14 July through 0000 UTC 18 July. RI to Emily would have occurred during that timeframe from LHCPE or other factors such as SST. Furthermore, an NHC report states Emily's winds peaked to Category-4 early on 7/15/2005 and Emily briefly became a Category-5 as well 0000 UTC 17 July about 100 n mi to the southwest of Jamaica (Franklin and Brown, 2006). Therefore, this study will conservatively

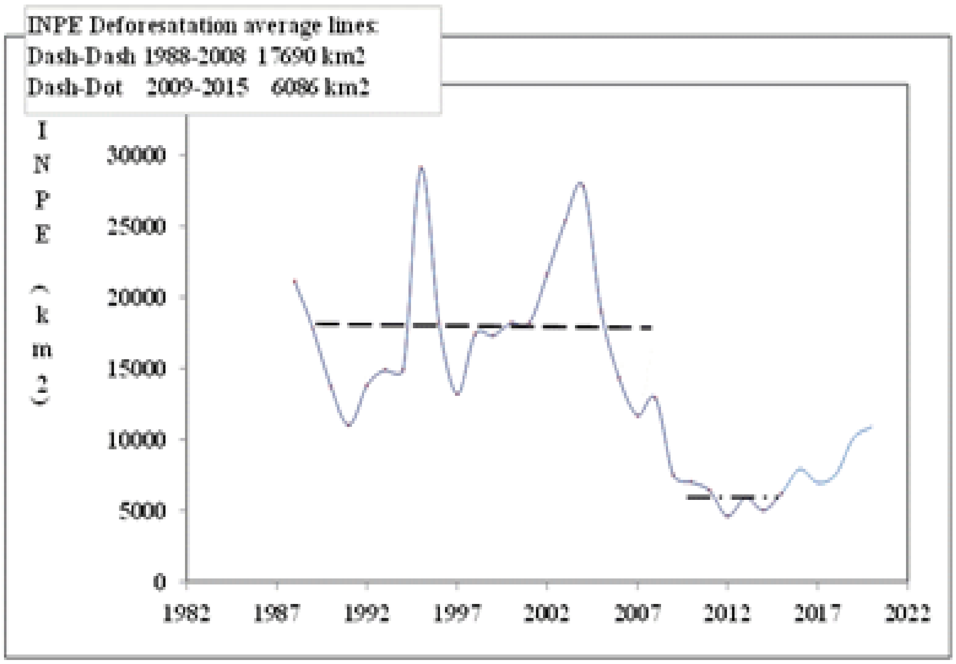

Figure 6. Raw INPE deforestation area (km^2).
Source: Frederick Kenneth Weiersmueller after INPE (2019) data.

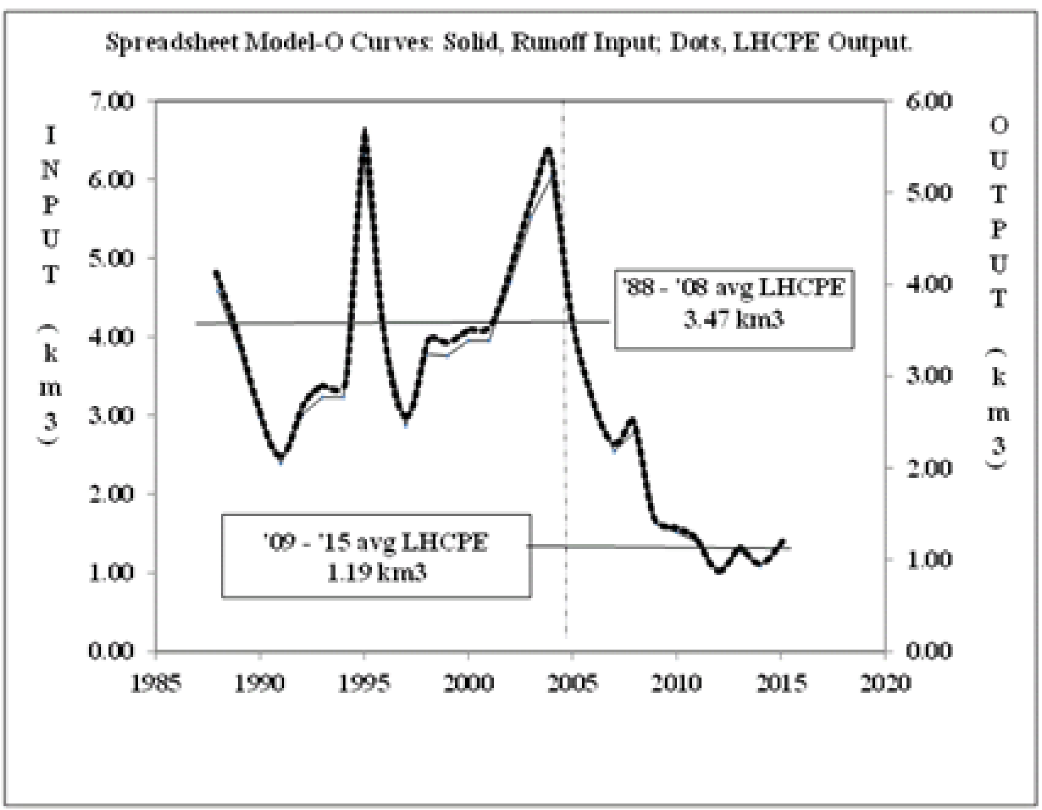

Figure 7. Spreadsheet Jun1-Nov30 deforestation Model-O input (km^3) and LHCPE calculated output (km^3).
Source: Frederick Kenneth Weiersmueller

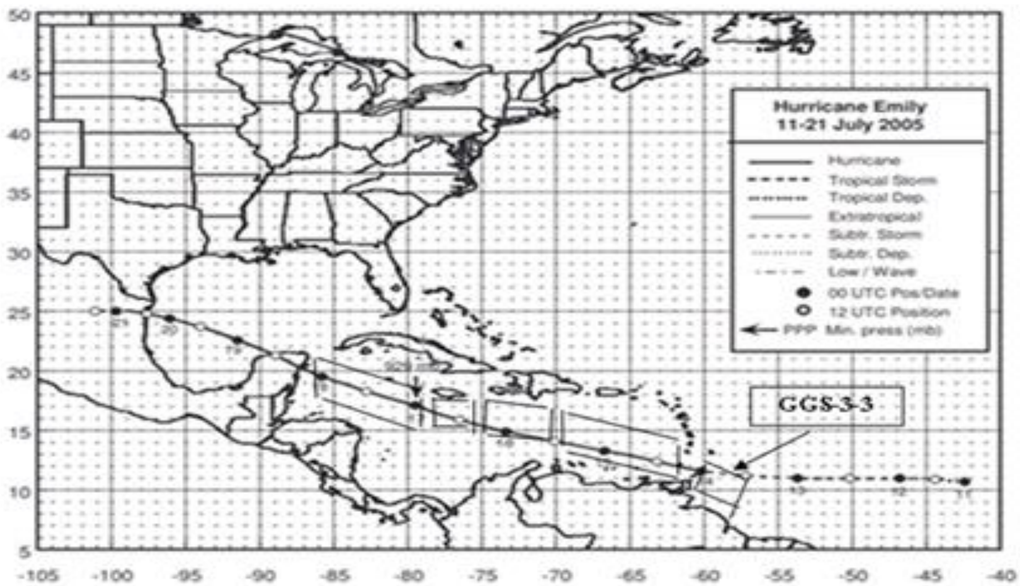

(a) Author GGS-4 annotations on Figure 1 of Franklin and Brown (2006).

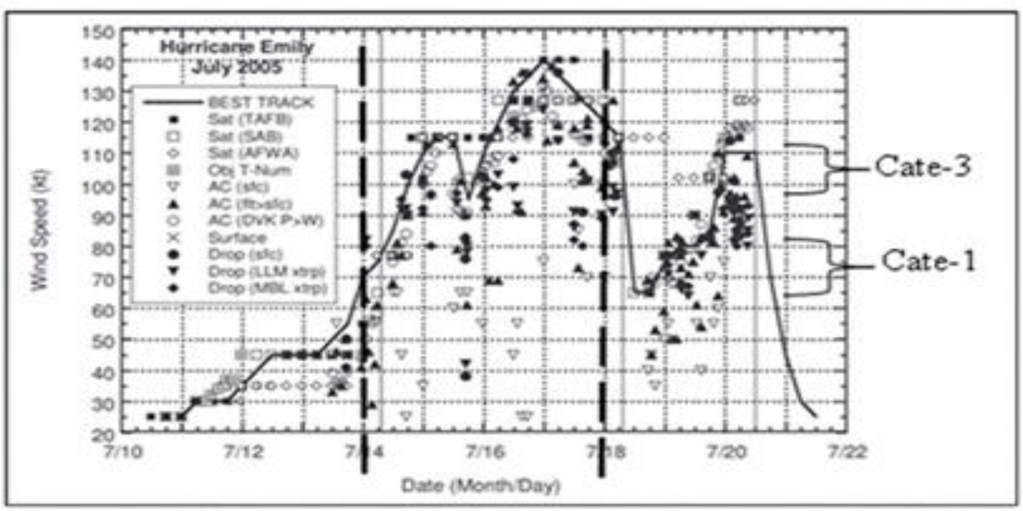

(b) Author annotations on Figure 2 of Franklin and Brown (2006).

Figure 8. (a) Emily's path and (b) Emily's wind speeds along that path.
Source: Frederick Kenneth Weiersmueller after (Franklin and Brown, 2006).

consider Emily as at least Category-3 for the entire GGS-4 area, during the four days, 7/14/2055 0000 UTC until 7/18/2005 0000 UTC. This study then analyzed the 2005 seasonal LHCPE attributed to GGS-4 during Emily's path from GGS-4-1 to GGS-4-4.

Seasonal LHCPE and maximum runoff flow during Emily's path through GGS-4

The arrow in Figure 9a points to the 1.06 km^3 Model-O-LHCPE that accumulated in GGS-4 during the hurricane season. Emily's path took it through the entire GGS-4, always maintaining Category-3 and above. That 1.06 km^3 LHCPE from GGS-4 is 28.4% of the 2005 seasonal 3.73 km^3 LHCPE calculated in column N. That significant seasonal LHCPE could have contributed to Emily's RI. In Figure 9b, this study looked at the heavy May-June runoff flow after Giffard et al. (2019). That is in relation to the typical GGS-n(-n) considering the typical 80 cm/sec Amazon runoff flow. Figure 9b illustrates that heavy May-Jun runoff flow interfacing Emily's path from 8/14-8/18 in 2005. Figure 9b depicts a hypothetical runoff floater, "X", on May 1 at the start of GGS-1, the discharge plume. The

(a)

	H	I	J	K	L	M	N	O	
		Model-A: All Amazon Runoff (Sect. B)			Model-O: Only Defor. Amazon Runoff (Sect. C)				
	LagTraEvap	Ruff Exhaust	LHCPE	Evap. Resid.	LagTraEvap	Ruff Exhaust	LHCPE	Evap. Resid	
		2566				413			
GGS-1	-9.3573	2564.0973	-8.4511	-0.9063	-0.0151	4.1413	-0.0136	-0.0015	2005
GGS-2	-112.2981	2676.3854	-101.4127	-10.9754	-0.1814	4.3226	-0.1635	-0.0176	
GGS-3	150.7812	2525.6043	136.1777	14.6036	0.2436	4.0791	0.2199	0.0236	INPE
GGS-4	726.6482	1798.9661	656.2706	70.3775	1.1736	2.9066	1.0599	0.1137	Deforest
GGS-5	196.7368	1602.2192	177.6824	19.0544	0.3178	2.5877	0.2870	0.0308	19000
GGS-6	33.9889	1568.2303	30.6970	3.2919	0.0549	2.5329	0.0496	0.0053	
GGS-7	15.3949	1562.8364	13.9039	1.4910	0.0249	2.5090	0.0225	0.0024	
GGS-8	504.6316	1048.2038	455.7568	48.9747	0.5150	1.6930	0.7361	0.0789	
GGS-9	889.5290	158.6748	803.3761	86.1529	1.4367	0.2563	1.2975	0.1391	
GGS-10	1147.9781	0.0001	143.3068	15.3680	1.8539	0.0001	0.2315	0.0248	
Totals:	3544		2307				3.73		

(b)

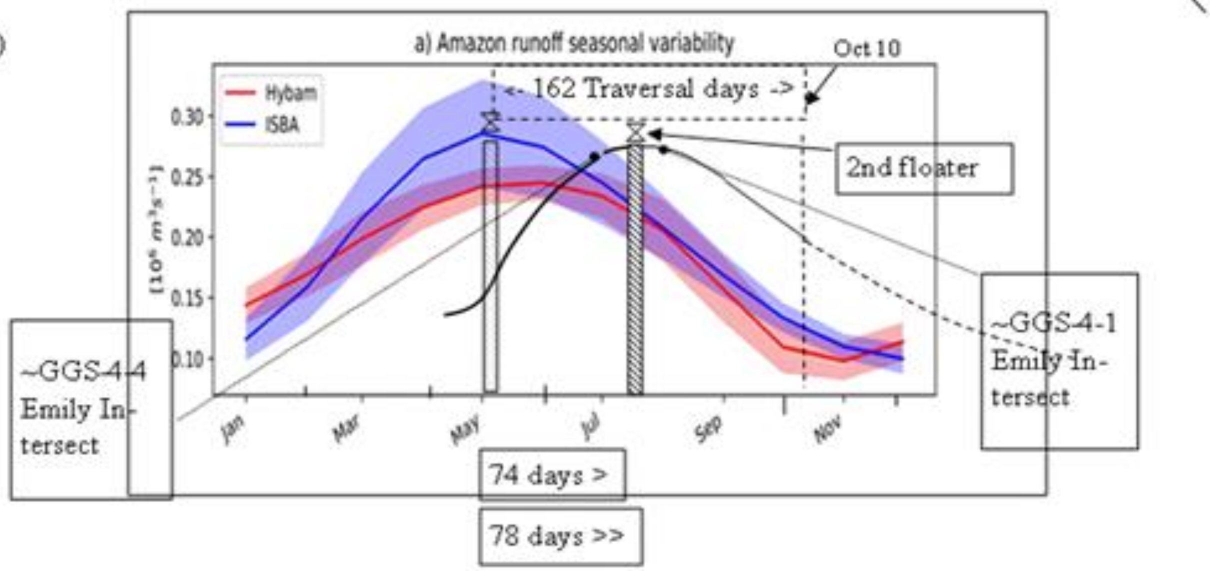

Figure 9. (a) 2005 Spreadsheet iteration excerpt and (b) Emily's available flow at GGS-4-2 midpoint, between 8/13 and 8/14 2005 after Giffard et al. (2019),
Source: (a) Frederick Kenneth Weiersmueller, (b) after Giffard et al. (2019).

second hypothetical runoff floater marks Emily's 4-day intersection with that May-June runoff flow. SMF indicates roughly 30 days of Amazon runoff flow within GGS-4. That allows four 7-day evaporation cycles, as per van der Ent and Tuinenburg (2017) to preset GGS-4 with significant LHCPE. Figure 9b also indicates the heavy flow at the approximate start of GGS-4-1 and it continues to the end of GGS-4-4 in Emily's timeframe, considering where the curve would be in each case. It is an important point that GGS-4 receives in mid-July through mid-October that heavier deforestation runoff flow from May through August as reported by Giffard et al. (2019). That runoff flow is approximately 0.27 m^3s^{-1}. That is 2.7 times the Dec-Apr flow of 0.10 m^3s^{-1} and again indicates possible RI from deforestation runoff. These heavy runoff volumes in Figure 9 occurring in Hurricane Emily's path, carried high percentages of the seasonal LHCPE km^3 and add weight to the argument that they contributed to Emily's RI. Interestingly, that LHCPE (km^3) from deforestation runoff possibly contributes RI during each hurricane season. It varies only as Amazon deforestation varies. Whereas, other RI phenomenon such as Atlantic Multidecadal Oscillation – Seas Surface Temperature (AMO-SST) and El Niño–Southern Oscillation (ENSO) Wind-Shear, may not be available for RI in each hurricane season.

DISCUSSION

SME summarizes all the 1988-2015 Spreadsheet iterations of Model-O output. It also summarizes all that output converted into 10^17 J/day as demonstrated in Table 1 for just the 2005 iteration. Figure 10 graphs those 1988-2015 Spreadsheet iterations of LHCPE converted to seasonal 10^17 J/day and their associated INPE. The years 1995, 2003, 2004 and 2005 are notable in Figure 10 for their high annual deforestation (km^2) and corresponding high LHCPE and 10^17 J/day. However, the question remains whether any of that 0.53 x 10^17

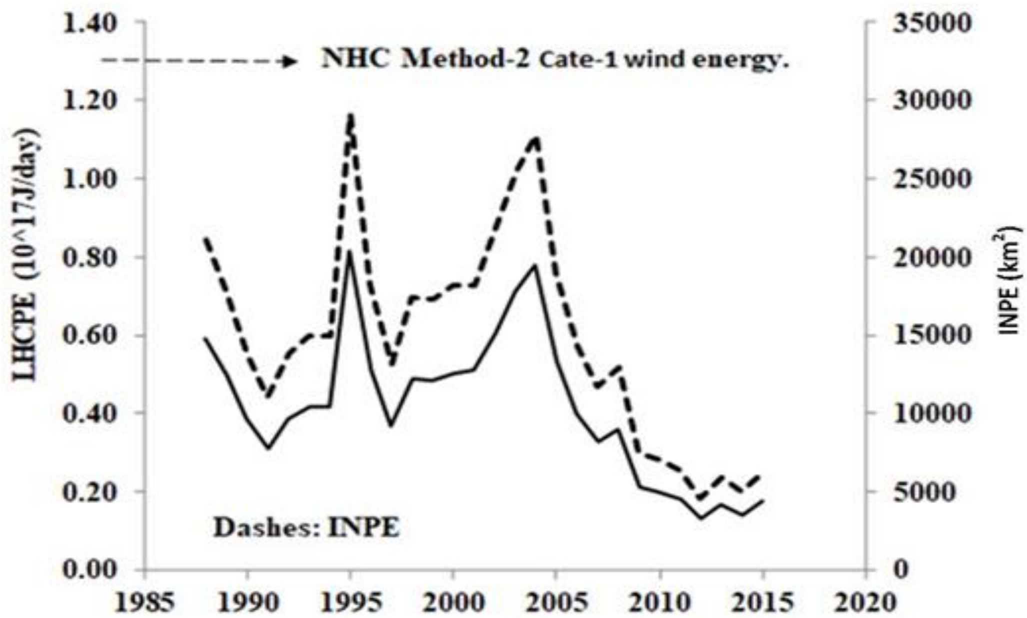

Figure 10. LHCPE converted from seasonal km^3 to 10^17 J/day and associated INPE, (2019).
Source: Frederick Kenneth Weiersmueller after INPE (2019).

J/day from Jun-Nov 2005-LHCPE intersected with the path of Emily in 2005 and did it cause intensification. Here this study will determine that. Table 2 is a special demonstration of the 2005, Table 1 calculations The Results section analyzed the "seasonal" LHCPE (km^3) of GGS-n(-n) which carried the max-runoff volumes that hurricane Emily could have utilized as RI. Here, this study breaks down that seasonal volume into "daily" contribution of LHCPE (10^17 J/day) towards RI of Emily in its Category-3 formation. Then LHCPE (10^17 J/day as a percentage of Category-3 hurricane wind energy in 10^17 J/day is calculated for each GGS-n(-n) in the path of the hurricane.

The Table 2 special iterations of Table 1 indicate LHCPE could have possibly contributed 5.82% of the 10^17 J/day towards Emily as a Category-3 hurricane in GGS-4.

However, so far the author had only considered 2005 INPE "fresh" deforestation – 19014 km2 for 2005 - and had not included the additional 113710 km2 from pasture reuse of deforested area from 1970 to 2004 (INPE, 2019). That totals instead 132724 (see SMG) for greater input to Model-O in 2005. Applying that increased deforested area to the Spreadsheet calculations (see SMD, SME, and SMG) yields 2.34 km3 of Model-O LHCPE output at GGS-4 instead of 1.6 km3. As a result, the special iteration of Table-1 in SMD indicates the LHCPE could have possibly contributed 12.85% towards Emily as a Category-3 hurricane in GGS-4, and more indication of possible RI.

A disparity may appear in that the 2.34 km3 Model-O LHCPE in GGS-4 is only 0.35% of the 656.27 km3 Model-A LHCPE in GGS-4 for 2005. The following analogy should clarify that. In this analogy, the 2.34 km3 contributes 12.85% to the areal formation (Emanuel, 1998) of a Category-3 hurricane from a Category-2 hurricane. The 656.27 km3 contributes 18% (see SMH for analogous calculation), to the volumetric formation (NHC, 2020) of a Category-1 hurricane from a tropical storm. The Category-1 volumetric formation from a tropical storm requires 5.2 x 10^19 J/day, whereas the Category-3 areal formation from a Category-2 requires a smaller 2.6 x 10^17 J/day.

In addition, the author notes this study conservatively applied the first meter down in Methodology regarding the 0.53 m3/m2 rate (consistent down to 10 meters) of deforested runoff after Bruno RD, et al.(2006). If deforestation drained soil water at 0.53 m3/m2 five meters down instead, then the Spreadsheet calculations would indicate even more RI. This study possibly represents the first time in the literature that hurricane RI analysis was tailored to the Amazon high runoff in the flooding season and its intersection with the hurricane season, Jun-Nov.

Other coexisting RI phenomenon

Studies have found other factors in the formation of these hurricanes. For example, an NHC report indicated Hurricane Denis had made portions of the Caribbean Sea warmer and hence more favorable for the development of hurricane Emily (Franklin, 2005).

However, this presentation calculates anthropologic

Table 2. The percent of daily LHCPE from GGS-4-n Model-O LHCPE resulting in RI to Hurricane Emily in 2005.

A	B	C	D	E	F	G	H	I	J
Assume Sprdsht Model-O LHCPE km3 = 10^12 kg	Assume Sprdsht Model-O LHCPE km3 = 10^12 kg	GGS-n LHCPE km3 Jun-Nov	B x C x 2569 kJ/kg =	D x 10^3 J/kJ =	E x 1/180 =	GGS-n-n LHCPE	Days in path of hurr.	G x H = GGS-n-n LHCPE 10^17 J/day	Col. I as % Cate-3 calc. by Emanuel (1998)*
		10^12 kg	10^12 kJ	10^3 J Jun-Nov	10^12 J/day	10^17 J/day			
GGS-4-1	0.350	1.06	953.05	953048.9	5294.72	0.0529	1	0.0529	2.04%
GGS-4-2	0.200	1.06	544.60	544599.4	3025.55	0.0303	1	0.0303	1.16%
GGS-4-3	0.150	1.06	408.45	408449.5	2269.16	0.0227	1	0.0227	0.87%
GGS-4-4	0.300	1.06	816.90	816889.1	4538.33	0.0454	1	0.0454	1.75%
Totals for Emily 4 days, 7/14/ to 7/18/2005, primarily Cate-3:							4	0.1513	5.82%
* Emanuel (1998) – wind energy, average hurricane @ 50 m/sec, Cate-3:								2.6 x 10^17 J/day	

Source: Frederick Kenneth Weiersmueller

LHCPE from deforestation as a possible RI factor. That LHCPE-RI may act alone or it may coexist with phases of other RI phenomenon that are intermittent. Proper treatment of other RI that are intermittent. or stand-alone phenomenon coexisting with LHCPE-RI requires another study.

Conclusion

This study advances the oceanographic and marine science state of knowledge in the following ways. This study quantifies evaporation from Amazon deforestation runoff over the Central/ North American Boundary currents (GGS) and its latent heat flux from condensation (LHCPE). This study utilized only six months of annual Amazon basin river runoff data (Giffard et al., 2019) and annual deforestation data (INPE, 2019). That June 1 through November 30 data is appropriate to a typical hurricane season (Goldstein, 2021). That demarcates the deforestation latent heat flux properly as a cause for RI. This study looked at a substantial timeframe of data, 1988-2015, twenty-eight years regarding that LHCPE. This study analyzed 2005 Hurricane Emily's RI from its path-interface with the Latent Heat of Condensation Potential Energy (LHCPE) from deforestation runoff to be significant in orders of magnitude. That RI could be additive or stand-alone regarding other RI phenomenon. The comparisons herein are by like terms and similar order of magnitude only. Emanuel (1998) indicates large quantities of latent heat flux are necessary to perform work on the air. Nonetheless, this study repeatedly points to Amazon deforestation runoff's difficult-to-assess role in RI. What exact proportion exists between the LHCPE quantified here and its RI (hurricane kinetic energy product) remains unsolved. A more complex mathematical analysis is necessary. This study's findings suggest future experiments. The first suggestion is a study quantifying stable oxygen-18 isotopes originating from Amazon deforestation-site runoff insertion, present in ocean hurricane atmosphere, via reconnaissance aircraft such as the Global Hawk drone. It is known that the stable oxygen isotopes differ in seawater versus in river water (Craig and Gordon, 1965). A reconnaissance aircraft study of that type could be definitive in assessing deforestation runoff percentages in hurricane atmospheres. The second suggestion relates to the calculation here of deforestation runoff as a factor in Meridional Overturning Circulation (MOC) slow down studies (Feng et al., 2014; Bryan, 1986; Rahmstorf, 2003). The precipitation that is resultant from deforestation runoff LHCPE (Lindsey, 2009) remains in the North Atlantic Ocean at the end of GGS-10. Would that additional volume of warmer water influence the tipping point towards Meridional Overturning Circulation Slow Down?

CONFLICT OF INTERESTS

The author has not declared any conflict of interests and is sole creator of this document.

REFERENCES

Artemis (2013). Artemis Catastrophe bonds, insurance linked securities, reinsurance capital & investment, risk transfer intelligence. Retrieved from: https://www.artemis.bm/ news/pcs-ups-sandy-industry-loss-estimate- to-18-75-billion-

close-to-current-reported-losses/
Balaguru K, Flotz GR, Leung LR (2018). Increasing Magnitude of Hurricane Rapid Intensification in the Central and Eastern Tropical Atlantic. Geophysical Research Letters. DOI: 10.1029/2018GL077597.
Balaguru K, Chang P, Saravanan R, Jang CJ (2012). The barrier layer of the Atlantic warmpool: formation mechanism and influence on the mean climate. Tellus A: Dynamic Meteorology and Oceanography, 64(1):18162. DOI: 10.3402/tellusa.v64i0.18162
Bruno RD, da Rocha HR, de Freitas HC, Goulden ML, Miller SD (2006). Soil moisture dynamics in an eastern Amazonian tropical forest. Hydrological Processes 20(12):2477-2489. DOI: org/10.1002/hyp.6211.
Bryan FO (1986). High-latitude salinity effects and interhemispheric thermohaline circulations. Nature 323:301-304. DOI: org/10.1038/323301a0
Chaves J. Neil N, Germer S, Neto SG, Krusche A, Elsenbeer H (2008). Land management impacts on runoff sources in small Amazon watersheds. Hydrological Processes 22(12):1766-1775. DOI: abs/10.1002/hyp.6803. 24.
Craig H, Gordon LI (1965). Deuterium and Oxygen 18 variations in the ocean and the marine atmosphere. Spoleto, Italy, Pisa, Consiglio nazionale delle richerche, Laboratorio de geologia nucleare. Retrieved from: https://www.semanticscholar.org/paper/Deuterium-and-oxygen-18-variations-in-the-ocean-and-Craig-Gordon/b803d3615c35b9c25d19fe88afd354f08368c085.
de Moraes JM, Schuler AE, Dunne T, Figueiredo RDO, Victoria RL (2006).Water storage and runoff processes in plinthic soils under forest and pasture in eastern Amazonia. Hydrological Processes 20(12):2509-2526. DOI: abs/10.1002/hyp.6213.
Eakins BW, Sharman GF (2010). Volumes of the World's Oceans from ETOPO1. Retrieved from: https://www.ngdc.noaa.gov/mgg/global/etopo1_ocean_volumes.html.
Emanuel KA (1998). The power of a hurricane: An example of reckless driving on the information superhighway. Massachusetts Institute of Technology - Kerry Emauel Professor of Atmospheric Science (website). Retrieved from: http://texmex.mit.edu/pub/emanuel/PAPERS/hurrpower.pdf; part of: https://emanuel.mit.edu/research-papers.
Feng QY, Viebahn JP, Dijkstra HA (2014). Deep ocean early warning signals of an Atlantic MOC collapse. Geophysical Research Letters 41(16):6008-6014. DOI: 10.1002/2014GL061019.
Findell KL Keys PW, van der Ent RJ, Lintner BR, Berg A, Krasting JP (2019). Rising Temperatures Increase Importance of Oceanic Evaporation as a Source for Continental Precipitation. Journal of Climate 32(22):7713–7726. DOI: 10.1175/JCLI-D-19-0145.1.
Franklin J(2005). Emily Discussion 8, National Hurricane Center, Miami, FL. Retrieved from: https://www.nhc.noaa.gov/archive/2005/dis/al052005.discus.008.sht ml.
Franklin JL, Brown DP (2006). Tropical Cyclone Synoptic Report-Hurricane Emily, National Hurricane Center, Miami FL. Retrieved from: https://www.nhc.noaa.gov/data/tcr/AL052005_Emily.pdf.
Giffard P, Llovel W, Decharm B (2019). Contribution of the Amazon River Discharge to Regional Sea Level in the Tropical Atlantic Ocean. Water 11(2348):16. DOI: 10.3390/w11112348.
Goldstein Z (2021). Atlantic & Eastern Pacific Climatology. National Hurricane Center Miami Fl. Retrieved from: https://www.nhc.noaa.gov/climo/#bac.
Goulding M, Barthem RB, Ferreura EJG (2003). The Smithsonian Atlas of the Amazon. Smithsonian Institute Press, Washington, DC. ISBN 10:1588341356 and ISBN 13: 9781588341358.
Gouveia NA, Gheradi DFM, Aragao LEOC (2019). The Role of the Amazon River Plume on the Intensification of the Hydrological Cycle. Geophysical Research Letters 46(21). DOI: 10.1029/2019GL084302.
Gray W (1981). Further analysis of tropical cyclone characteristics from rawinsonde compositing techniques. Monterey(CA): Naval Environmental Prediction Research Facility (U.S.). Retrieved from: https://apps.dtic.mil/dtic/tr/fulltext/u2/a102053.pdf.
Hence DA, Houze RA (2012). Vertical Structure of Tropical Cyclone Rainbands as seen by the TRMM. Journal of the Atmospheric Sciences pp. 2644-2661. 10.1175/JAS-D-11-0323.1.
HurricaneHuntersAssoc (NHC) (2020). How much Energy does a Hurricane Produce? Retrieved from: https://www.aoml.noaa.gov/hrd-faq/#hurricane-energy-production.
Instituto Nacional de Pesquisas Espaciais (INPE) (2019). National Institute for Space Research (Instituto Nacional de Pesquisas Espaciais INPE) p/o PRODES (Deforestation) Accumlated Deforestation Rates per Year in the Legal Amazon States, orig. 1985). Retrieved from: http://terrabrasilis.dpi.inpe.br/app/dashboard/deforestation/biomes/legal_amazon/rates.
Lindsey R (2009). Climate and Earth’s Energy Budget. Retrieved from: https://earthobservatory.nasa.gov/features/EnergyBalance.
Mariano A (2016). Surface Currents in the Atlantic Ocean. Retrieved from: http://oceancurrents.rsmas.miami.edu/atlantic/atlantic.html.
MarianoArrowData (2016). Ocean Surface Currents, Data. Retrieved from https://oceancurrents.rsmas.miami.edu/data.html.
Met (2021). How does the tropical cyclone obtain its energy? UK Meter.Serv. Retreived from: https://www.metoffice.gov.uk/research/weather/tropical-cyclones/facts#How%20do%20TCs%20form
NOAAFastFacts (2013). Coastal Fast Facts, s.l.: Office of Coastal Management. Retrieved from: https://coast.noaa.gov/data/nationalfacts/pdf/hand-out-coastal-fast-facts.pdf.
PRODES Amazon (2020). Earth Observation INPE. Retrieved from: http://www.obt.inpe.br/OBT/assuntos/programas/amazonia/prodes.
Rahmstorf S(2003). The Current Climate. Nature 421:699. DOI: 10.1038/421699a.
Raven PH, Berg LR (2006). Environment. John Wiley and Sons, NJ. ISBN: 10:0471704385 and ISBN 13: 9780471704386.
Ritchie H, Rose M (2019). Land Use. Retrieved from: https://ourworldindata.org/land-use.
Rogers RR, Yau MK(1989). A Short Course in Cloud Physics. Vol: 113, 3rd ed. Oxford and New York, Pergamon Press. ISBN: 0-7506-3215-1.
Saffir H, Simpson R (1973). Saffir-Simpson Hurricane Scale. Retrieved from: https://en.wikipedia.org/wiki/Saffir%E2%80%93Simpson_scale; and also https://www.weather.gov/mfl/saffirsimpson.
Shiklomanov IA(1998). Water Resources: A New Appraisal and Assessment for the 21st Century, UNESCO. DOI: org/10.1080/02508060008686794
Trenberth KE, Smith L, Qian T, Dai A, Fasulo J (2007). Estimates of Global Water Budget and Its Annual Cycle Using Observational and Model Data. Journal of Hydrometeorolgy 8(4):758-769. DOI: org/10.1175/JHM600.1.
Tuinenburg OA, Hutjes RWA, Kaba P (2012). The fate of evaporated water from the Ganges basin. Journal of Geophysical Research 117(D1). DOI: 10.1029/2011JD016221.
van der Ent RJ, Savenije HHG (2013). Oceanic Sources for Continental Precipitation. Water Resources Research 49(7):3993-4004. DOI: 10.1002/wrcr.20296/pdf.
van der Ent RJ & Tuinenburg OA (2017). The residence time of water in the atmosphere revisited. Hydrology and Earth System Sciences 21(2):779-790. DOI:10.5194/hess-21-779-2017.
Vizy EK, Cook KH (2010). Influence of the Amazon/Orinoco Plume on the summertime Atlantic climate. Journal of Geophysical Research 115(D21112):1-18. DOI: 10.1029/2010JD014049.
WikipediaLongitude (2019). Length of a degree of longitude. Retrieved from: https://en.wikipedia.org/wiki/Longitude.
Wunsch C (2005). The Total Meridional Heat Flux and Its Oceanic and Atmospheric Partition. Journal of Climate 18(21):4374-4380.
Zehnder JA (2020). Anatomy of A Cyclone, https://www.britannica.com/science/tropical-cyclone.

Supplementary Materials (SM)

Determining GGS Currents Surface Areas.

Geometric analysis for each GGS-n (W or L meas. by curvy Arrows, Lat. or Long).	fx Factor	W	H	W (km)	L (km)	GGS sub km2	GGS Total km2	SAC Sect. A Factor	GGS-n-n % of Total
GGS-1									
Dsch. Plume, trpzd. b1=10, b2=6, h=.75	0.5	16	0.75	1600	75	60000	60000	0.000166	
GGS-2									
North Brazil, (prllgrm)	1	18	4	1800	400	720000	720000	0.001994	
starts 33o W 7o S, ends 6o N 50oW									
GGS-3									
(-1) Guiana(a), triangle	0.5	2	6	200	600	60000			
(-2) Guiana(b), prllgrm	1	3	6	300	600	180000			
(-3) Guiana(c), prllgrm, ends 14o N 62o W.	1	3	4	300	400	120000	360000	0.000997	
GGS-4									
(-1) Carib.(a), rectangle	1	4	7	400	700	280000			0.350
(-2) Carib.(b), rectangle	1	2	8	200	800	160000			0.200
(-3) Carib.(c), square, ends 79o W	1	4	3	400	300	120000			0.150
(-4) Carib.(d) prllgrm, ends 85o W.	1	6	4	600	400	240000	800000	0.002216	0.300
GGS-5									
(-1) Loop(a), rectangle, starts at 22o N, ends 26°N 88°W	1	2	4	200	400	80000			
(-2) Loop(b), rectangle, ends 83°W	1	1	2	100	200	20000			
(-3) Loop(c), triangle, ends 82o W	0.5	2	2	200	200	20000	120000	0.000332	
GGS-6									
Florida; Key West to Miami, rctngl, ends 80oW	1	0.5	4	50	400	20000	20000	0.000055	
GGS-7									
Florida; Miami to Jcksv. Rectangle; ends 30o N.	1	0.25	3.5	25	350	8750	8750	0.000024	
GGS-8									
(-1) Jcksv. to Beaufort, SC.(a); Triangle;	0.5	3	4	300	400	60000			
(-2) Beaufort, SC to Cape Hat.(b); trpzd., b1=4, b2=8, h=3;	0.5	12	3	1200	300	180000	240000	0.000665	
GGS-9									
(-1) Cape to 70o W(a); trpzd.; a=8, b1=2.5, b2=6, h=2.5;	0.5	8.5	2.5	850	250	106250			
(-2) 70o W to 60oW(b) prllgrm , a=2.5, b=6, h=2.5;	1	3	9	300	900	270000	376250	0.001042	
GGS-10									
60o W to 48o W; rectangle;	1	12	4	1200	400	480000	480000	0.001330	
Total km2:							3185000		

approx. GGS traversal length in northward direction	
GGS 1	750
GGS 2	1800
GGS 3-1	600
GGS 3-2	600
GGS 3-3	400
GGS 4-1	700
GGS 4-2	800
GGS 4-3	300
GGS 4-4	400
GGS 5-1	400
GGS 5-2	200
GGS 5-3	200
GGS 6	400
GGS 7	350
GGS 8-1	200
GGS 8-2	200
GGS 9-1	800
GGS 9-2	900
GGS 10	1200
GGS Len.	11200

A. Determining GGS Currents Surface Areas

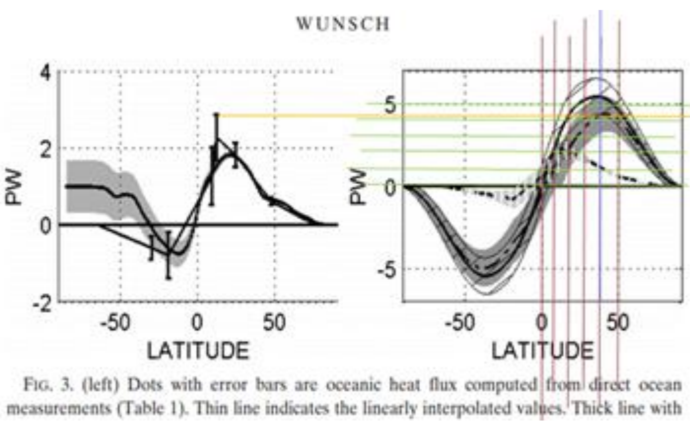

GGS-n	N Lat	PW (or x 10^15 W)
1	1	-0.20
2	1	-0.20
3	8.5	0.80
4	16	1.60
5	24	2.90
6	25	3.00
7	27	3.10
8	33	3.70
9	37	4.15
10	40	4.20
		REC Factor

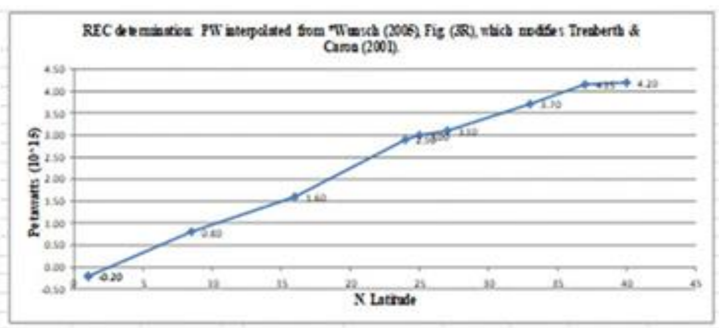

B. REC Interpolation (left) with annotations after Figure-3-Right of Wunsch C (2005); author's corresponding worksheet (right).

VAN DER ENT AND SAVENIJE: PRECIPITATION AND CORRELATION WITH SST

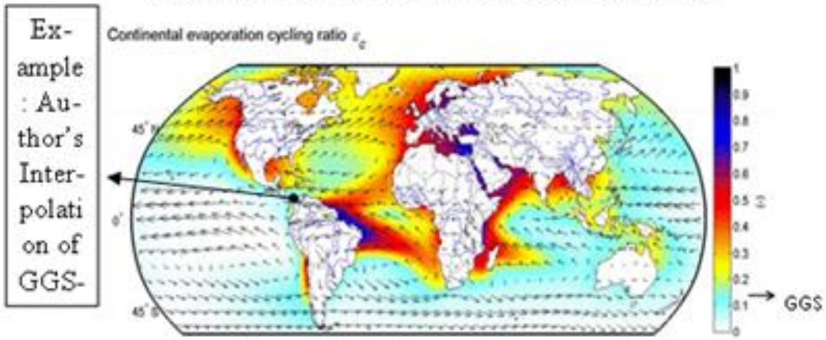

Figure 1. The continental evaporation cycling ratio ε_c (equation (4)). This is the fraction of the evaporation that is transported to, and precipitates on, continents. These data are obtained from backward tracking the precipitation on the continents. The data are for the period 1990-2009 and displayed for oceanic regions only. See *van der Ent et al.* [2010] for the values on the continents themselves. The arrows indicate the horizontal moisture flux field.

GGS-N	1	2	3	4	5	6	7	8	9	10
Cycling Ratio	0.75	0.75	0.70	0.13	0.35	0.30	0.25	0.25	0.18	0.28

Table 1 assumes the following. A km3 of H2O equals 10^12 kg of H2O. Hurricanes form up to 15 km high (HurricaneHuntersAssoc, 2020). There is a wide range of temperatures at which condensation of clouds occurs. Those were from altitudes between 2400 m and 15000 m with temperatures ranging from 24 ° C to -70 ° C respectively (Schlesinger WH & Bernhardt ES, 2013). A study (Rogers RR & Yau MK, 1989) calculated the specific latent heat for condensation of water in clouds at various altitudes: 2694 kJ/kg Latent heat of Cond of H2O at 15000 m and -70 deg C; 2444 kJ/kg Latent heat of Cond at 2400 m and 24 deg C. From those figures the author calculated an average of 2569 kJ/kg for the altitude range. The author used that as a constant in Table 3, column C.

C. Interpolation (left) of GGS-n EvapTranInlndCyc Ratio Figure 1 (van der Ent RJ et al., 2013); and determination (right) of Table 1 2569 kJ/kg constant.

Special Iteration of Table-1 to determine % of daily GGS-4-n LHCPE in 2005 became RI to Emily.

A	B	C	D	E	F	G	H	I	
Assume Spd:ht H2O km3=10^12 kg H2O	GGS-n-n to GGS-n ratio	GGS-n4 LHCPE km3 (jun-nov) =	B x C x 2569 kJ/kg =	D x 10^3 J/kJ =	E x 1/180 =	GGS-n-n LHCPE	Days in path of hurr	G x H = GGS-n-n LHCPE 10^17 J/day	Column I as % Case-3 calc. by Emanuel (1995) *
GGS-n(-n)		10^12 kg	10^12 kJ	10^12 J (jun-nov)	10^12 J/day	10^17 J/day			
E GGS-4-1:	0.350	2.34	2104.01	2104011	11688.95	0.1169	1	0.1169	4.50%
E GGS-4-2:	0.200	2.34	1202.29	1202292	6679.40	0.0668	1	0.0668	2.57%
E GGS-4-3:	0.150	2.34	901.72	901719	5009.55	0.0501	1	0.0501	1.93%
E GGS-4-4:	0.300	2.34	1803.44	1803438	10019.10	0.1002	1	0.1002	3.85%
		(Totals: Emily 4 days, 7/14 to 7/18/2005, primarily Case-3)					4	0.3340	12.85%

* Emanuel (1995) - wind energy, average-hurricane @ 50 m/sec Case-3 : 2.6 10^17 J/day

2005 Spreadsheet for 132724 km2 raw INPE

Model-O: Only Defor. Amazon Runoff (Sect. C)

L	M	N	O	
Lag Tr of Evap	Runff. Exhaust.	LHCPE	Evap. Resid.	
Inputs ->	9.10			
-0.0333	9.1333	-0.0301	-0.0032	2005
-0.4000	9.5333	-0.3612	-0.0387	
0.5371	8.9962	0.4851	0.0520	INPE
2.5883	6.4079	2.3376	0.2507	Deforest.
0.7008	5.7071	0.6329	0.0679	132724
0.1211	5.5860	0.1093	0.0117	Pasture
0.0548	5.5312	0.0495	0.0053	Reuse
1.7975	3.7337	1.6234	0.1741	
3.1685	0.5652	2.8616	0.3069	
4.0887	0.0001	0.5105	0.0547	
		8.22	0.8814	
		8.22	0.88	

D. Special Iteration of Table 1 using 2.34 km3 as input (left). Spreadsheet iteration calculating 2.34 km3 Model-O-LHCPE output at GGS-4 (right). See also SM. E and SM. G.

	Results - Spreadsheet Iterations						Discussion - Spreadsheet Iterations		
	Model A			Model O					
	Runoff Raw Data		Conv. to Init. Input (Col. I)	Deforest. Raw Data (INPE)	Conv. To Init. Input (Col. M)	LHCPE (Col. N)	LHCPE (Col. N)	% of NHC Meth. 2 Category 1	% of Emanuel (1998) Category 3
	Giffard (ISBA)	Conv. to				GGS Total	Conv. to J/day		
yyyy	10^6 m3/sec	km3/yr	km3/seas.	km2/yr	km3/seas	km3/seas	10^17 J/day fx		
1988	0.196	6182	2782	21100	4.58	4.14	0.59	45.4	22.7
1989	0.221	6970	3137	17800	3.87	3.49	0.50	38.3	19.2
1990	0.195	6150	2768	13700	2.98	2.69	0.38	29.5	14.8
1991	0.198	6245	2810	11000	2.39	2.16	0.31	23.7	11.8
1992	0.142	4479	2015	13800	3.00	2.71	0.39	29.7	14.9
1993	0.210	6623	2981	14900	3.24	2.92	0.42	32.1	16.0
1994	0.193	6087	2739	14900	3.24	2.92	0.42	32.1	16.0
1995	0.180	5677	2555	29100	6.32	5.71	0.81	62.7	31.3
1996	0.191	6024	2711	18200	3.95	3.57	0.51	39.2	19.6
1997	0.185	5835	2626	13200	2.87	2.59	0.37	28.4	14.2
1998	0.140	4416	1987	17400	3.78	3.41	0.49	37.5	18.7
1999	0.190	5993	2697	17300	3.76	3.39	0.48	37.3	18.6
2000	0.213	6718	3023	18200	3.95	3.53	0.50	38.8	19.4
2001	0.200	6308	2839	18200	3.95	3.57	0.51	39.2	19.6
2002	0.198	6245	2810	21600	4.69	4.24	0.60	46.5	23.3
2003	0.189	5961	2682	25400	5.52	4.98	0.71	54.7	27.3
2004	0.188	5930	2668	27800	6.04	5.45	0.78	59.9	29.9
2005	0.180	5677	2555	19014	4.13	8.22	1.17	90.2	45.1
2006	0.219	6907	3108	14300	3.11	2.80	0.40	30.7	15.4
2007	0.193	6087	2739	11700	2.54	2.29	0.33	25.2	12.6
2008	0.221	6970	3137	12900	2.80	2.53	0.36	27.8	13.9
2009	0.233	7349	3307	7500	1.63	1.47	0.21	16.1	8.1
2010	0.170	5362	2413	7000	1.52	1.37	0.20	15.1	7.5
2011	0.202	6371	2867	6400	1.39	1.26	0.18	13.8	6.9
2012	0.204	6434	2895	4600	1.00	0.90	0.13	9.9	5.0
2013	0.200	6308	2839	5900	1.28	1.16	0.17	12.7	6.4
2014	0.207	6529	2938	5000	1.09	0.98	0.14	10.8	5.4
2015	0.186	5866	2640	6200	1.35	1.22	0.17	13.4	6.7
2016				7900	1.72				
2017				6947	1.51				
2018				7536	1.64				
2019	No Giffard (2019) data past 2015.			10100	2.19				
2020				10900	2.37				
2021				13000	2.82				
	Avgs.	1988-2015	2760	13838	3.21	3.06	0.44	33.59	16.79
		1988-2008	2732	17691	3.84	3.68	0.53	40.42	20.21
		2009-2015	2843	6086	1.32	1.19	0.17	13.10	6.55
		2016-2021		9397					
Spreadsheet Iteration of Deforestation Pasture Reuse of 1970-2004 plus the 2005 deforesetation.									
70-'04	0.180	5677	2555	134724	29.26	i.e. per Giffard, 2019 and Bruno, 2006.			
70-'04, PastReuse Runoff = 29.26 km3 w/o 17%, or					4.97	km3 adjusted per 17%, (Chaver, 2008)			
		4.97 km3 plus 2005 "4.13" km3 =			9.10	km3 of Spreadsheet Model-O Initial Input.			

E. Summary of 1988-2015 Spreadsheet Iterations (includes iterations of Table-1, 10^17 J/day conversions). Also calculation of 9.10 km3 (bottom) Initial Input to Model-O Spreadsheet iteration for 1970-2004 pasture reuse areas (de Moraes et al., 2006) and (Chaves et al., 2008).

Analysis: GGS-n transversal days.

Constants: 86.4 x 10^3 sec/day; GGS avg. vel. = 80 cm/sec or 10^-5 km/sec; 1

Input: (km) -->	11200	km /	80	10^-5 km/sec	eqs	14000000	trav. Sec
14000000	trav. Sec /	86400	sec/day	eqs	162.037	trav. day(s)	

GGS-n km2	GGS-n	GGS Traverse Days
750	GGS 1	10.85
1800	GGS 2	26.04
1600	GGS 3	23.15
2200	GGS 4	31.83
800	GGS 5	11.55
400	GGS 6	5.79
350	GGS 7	5.06
400	GGS 8	5.79
1700	GGS 9	24.60
1200	GGS 10	17.37
11200		162.02

	sub trvs km	GGS-n trvs. km	sub trv days	GGS-n trv days
GGS 1	750	750		10.85
GGS 2	1800	1800		26.04
GGS 3-1	600		8.68	
GGS 3-2	600		8.68	
GGS 3-3	400	1600	5.79	23.15
GGS 4-1	700		10.13	
GGS 4-2	800		11.55	
GGS 4-3	300		4.34	
GGS 4-4	400	2200	5.79	31.83
GGS 5-1	400		5.79	
GGS 5-2	200		2.89	
GGS 5-3	200	800	2.89	11.55
GGS 6	400	400		5.79
GGS 7	350	350		5.06
GGS 8-1	200			
GGS 8-2	200	400	2.89	5.79
GGS 9-1	800		11.57	
GGS 9-2	900	1700	13.02	24.60
GGS 10	1200	1200		17.37
Total:	11200			162.02

F. Analysis of GGS-n(-n) Amazon runoff traversal days northward.

Deforestation km2 plus prior-year Pasture Reuse of Deforested km2 in Amazon Basin						
Note: Increasing Sum of Reuse deforestation runoff, km2, is per (Chaves J, et al., 2008), (de Moraes JM, et al., 2006);- calculation below, which assumes 1 yr. to develop pasture; INPE data from 1970 to 1988 were averaged prior to annual satellite recordkeeping starting 1988 (INPE, 2019); assumes 100% reuse of deforested areas.						
A	B	C	D	E	F	G
yyyy	Deforest. of Curr-Yr (km2)	Defor. of Prev-Yr becomes Pasture Reuse (km2)	17% runoff Past. Reuse	C X D	Increasing Sum of Runoff from Reuse (km2)	B + F Total Deforest. Runoff area per Year (km2)
1969	0	0	0	0.00	0.00	0
1970	18016	0	0.17	0.00	0.00	18016
1971	18016	18016	0.17	3063	3063	21079
1972	18016	18016	0.17	3063	6125	24141
1973	18016	18016	0.17	3063	9188	27204
1974	18016	18016	0.17	3063	12251	30267
1975	18016	18016	0.17	3063	15314	33330
1976	18016	18016	0.17	3063	18376	36392
1977	18016	18016	0.17	3063	21439	39455
1978	21130	18016	0.17	3063	24502	45632
1979	21130	21130	0.17	3592	28094	49224
1980	21130	21130	0.17	3592	31686	52816
1981	21130	21130	0.17	3592	35278	56408
1982	21130	21130	0.17	3592	38870	60000
1983	21130	21130	0.17	3592	42462	63592
1984	21130	21130	0.17	3592	46054	67184
1985	21130	21130	0.17	3592	49646	70776
1986	21130	21130	0.17	3592	53239	74369
1987	21130	21130	0.17	3592	56831	77961
1988	21050	21130	0.17	3592	60423	81473
1989	17770	21050	0.17	3579	64001	81771
1990	13730	17770	0.17	3021	67022	80752
1991	11030	13730	0.17	2334	69356	80386
1992	13786	11030	0.17	1875	71231	85017
1993	14896	13786	0.17	2344	73575	88471
1994	14896	14896	0.17	2532	76107	91003
1995	29059	14896	0.17	2532	78640	107699
1996	18161	29059	0.17	4940	83580	101741
1997	13227	18161	0.17	3087	86667	99894
1998	17383	13227	0.17	2249	88916	106299
1999	17259	17383	0.17	2955	91871	109130
2000	18226	17259	0.17	2934	94805	113031
2001	18165	18226	0.17	3098	97903	116068
2002	21651	18165	0.17	3088	100991	122642
2003	25396	21651	0.17	3681	104672	130068
2004	27772	25396	0.17	4317	108989	136761
2005	19014	27772	0.17	4721	113710	132724

G. Calculation of Increasing Sum of Reuse Deforestation km2, see SM.D and SM.E.

A	B	C	D	E	F	G	H	I	J
assume Sprdsht Model-O LHCPE km3 = 10^12 kg	GGS-n-n to GGS-n ratio	GGS-n LHCPE km3 Jun-Nov	B x C x 2569 kJ/kg =	D x 10^3 J/kJ =	E x 1/180 =	GGS-n-n LHCPE	Days in path of hurr.	G x H = GGS-n-n LHCPE 10^17 J/day	Col. I as % NHC Method-1 Gray (1981)*
		10^12 kg	10^12 kJ	10^12 J Jun-Nov	10^12 J/day	10^17 J/day			
GGS-4-1	0.35	656.27	590085.17	590085171	3278250.95	32.7825095	1	32.782509	6.30%
GGS-4-2	0.2	656.27	337191.53	337191526	1873286.26	18.7328626	1	18.732863	3.60%
GGS-4-3	0.15	656.27	252893.64	252893645	1404964.69	14.0496469	1	14.049647	2.70%
GGS-4-4	0.3	656.27	505787.29	505787289	2809929.38	28.0992938	1	28.099294	5.40%
Totals for Emily 4 days, 7/14/ to 7/18/2005, primarily Cate-3:							4	93.664313	18.01%

* Gray (1981) – total wind energy, inner to outer wall average hurricane @ 50 m/sec, Cate-1: 5.2 x 10^19 J/day

H. Special iteration of Table 2. The percent of daily Model-A-LHCPE from GGS-4 resulting in RI considering NHC Method-1 (Gray 1981).